Chemistry
A European
Journal

Chemistry Europe
European Chemical Societies Publishing

Accepted Article

Title: Solubility-Driven Isolation of a Metastable Nonagold Cluster with Body-Centered Cubic Structure

Authors: Hui Shen, Elli Selenius, Pengpeng Ruan, Xihua Li, Peng Yuan, Omar Lopez-Estrada, Sami Malola, Shuichao Lin, Boon K. Teo, Hannu Häkkinen, and Nanfeng Zheng

To be cited as: *Chem. Eur. J.* 10.1002/chem.202001753

Link to VoR: https://doi.org/10.1002/chem.202001753

WILEY-VCH

10.1002/chem.202001753

WILEY-VCH

RESEARCH ARTICLE

Solubility-Driven Isolation of a Metastable Nonagold Cluster with Body-Centered Cubic Structure

Hui Shen,[1] Elli Selenius,[2] Pengpeng Ruan,[1] Xihua Li,[1] Peng Yuan,[1] Omar Lopez-Estrada,[2] Sami Malola,[2] Shuichao Lin,[1] Boon K. Teo, [1] Hannu Häkkinen, [*,2] Nanfeng Zheng[*,1]

Abstract: The conventional synthetic methodology of atomically precise gold nanoclusters using reduction in solutions offers only thermodynamically most stable nanoclusters. We report herein a solubility-driven isolation strategy to access the synthesis of a metastable gold cluster. The cluster, with the composition of $[Au_9(PPh_3)_8]^+$ (**1**), displays an unusual, nearly perfect body-centered-cubic (bcc) structure. As revealed by ESI-MS and UV/Vis measurement, the cluster is metastable in solution and converts to the well-known $[Au_{11}(PPh_3)_8Cl_2]^+$ (**2**) within just 90 min. DFT calculations revealed that while both **1** and **2** are eight-electron superatoms, there is a driving force to convert **1** to **2** as shown by the increased cohesion and larger HOMO-LUMO energy gap of **2**. The isolation and crystallization of the metastable gold cluster were achieved in a biphasic reaction system in which reduction of gold precursors and crystallization of **1** took place concurrently. This synthetic protocol represents a successful strategy for investigations of other metastable species in metal nanocluster chemistry.

Introduction

In the recent decades, great efforts have been made in the synthesis and characterization of atomically precise gold nanoclusters.[1] Some representative examples are phosphine-stabilized Au_{11},[2] Au_{13},[3] Au_{39},[4] thiol-protected Au_{25},[5] Au_{102},[6] Au_{144}[7] alkynyl-capped Au_{25},[8] Au_{144},[9] and N-heterocyclic carbene-stabilized Au_{13},[10] Au_{25}[11] et al. respectively. The most commonly used synthetic method is the so-called bottom-up approach.[12] The key principle in this strategy, as summarized by Jin, Tsukuda, Konishi, and many others, is the "survival of the robustest", which means products obtained are, in general, the most stable one among various factors such as sizes, compositions, morphologies, and structures.[13]

This principle is understandable when one retrospects the conventional bottom-up route for preparing gold nanoclusters (NCs) (Figure S1).[14] For the synthesis, it mainly involves three steps: 1. Reduction, in which metal ions are reduced in the presence of stabilizer to produce NCs; 2. Aging, whose function is to transform the unstable species into stable ones; 3. Isolation, which further purifies the stable ones. In other words, the products obtained in conventional synthetic protocols are generally the thermodynamically most stable ones.

On the other hand, access to metastable species is often critical in the understanding of chemical principles in the formation, transformation and functionalization of materials. Such access, however, remains as a great challenge in ligated atomically precise gold NCs, because, during the conventional reduction-aging-isolation process, the conversion from metastable species to stable ones will take place spontaneously. It is noteworthy that nowadays some advanced techniques such as electrospray ionization mass (ESI-MS) and nuclear magnetic resonance (NMR) can help track the intermediates of NCs formation, but it seems powerless for probing their exact structure information.[15] It is, thus, of urgency to devise a new methodology for crystallizing metastable gold NCs. In this context, we rationalize that by decreasing the reaction rate and shortening the aging time, it may be possible to trap metastable NCs in the reduction-aging-isolation process.

Herein, we describe a biphasic reaction system that allows the stabilization and crystallization of metastable gold NCs. The principle in this synthetic protocol is that after the formation of metastable intermediates, they were arrested by encapsulating with a "poor" solvent (low solubility) and extracted from the reaction immediately, which stops any further transformation. This approach allows trapping a highly reactive gold cluster with the composition of $[Au_9(PPh_3)_8]Cl$ (**1**). The product was characterized by single-crystal X-ray crystallography, ESI-MS, ultraviolet/visible (UV/Vis), NMR, and DFT calculation. Our results showed that the structure and property of metastable clusters could be quite different from stable ones in terms of body-centered cubic (bcc) architecture and fast-transformation feature of present one. The synthesis and detailed structural characterization of the metastable gold cluster in this work represents a conceptional strategy for access to many other metastable metal NCs.

Results and Discussion

Synthesis of 1. Shown in Figure 1 is the design principle for the isolation and crystallization of metastable gold NCs. In the initial step, metal precursor, organic ligand, and a weak reducing agent are mixed together in a solvent to form a homogenous solution.

[a] H. Shen, P. Ruan, X. Li, P. Yuan, Dr. S. C. Lin, Prof. B. K. Teo, Prof. N. F. Zheng
State Key Laboratory for Physical Chemistry of Solid Surfaces, Collaborative Innovation Center of Chemistry for Energy Materials, and National & Local Joint Engineering Research Center for Preparation Technology of Nanomaterials, College of Chemistry and Chemical Engineering, Xiamen University
Xiamen 361005, China
E-mail: nfzheng@xmu.edu.cn

[b] E. Selenius, O. Lopez-Estrada, Dr. S. Malola, Prof. H. Häkkinen
Departments of Physics and Chemistry, Nanoscience Center, University of Jyväskylä FI-40014 Jyväskylä, Finland

E-mail: hannu.j.hakkinen@jyu.fi

Supporting information for this article is given via a link at the end of the document.

10.1002/chem.202001753
WILEY-VCH

RESEARCH ARTICLE

In sharp contrast to the conventional synthesis that crystallization process was done after the aging step, in present situation, a solvent with a poor solubility for the cluster products was layered over the reaction mixture (tube a in Figure 2) prior to the reduction and aging process. As devised, metal precursors are reduced slowly to form metastable clusters in the

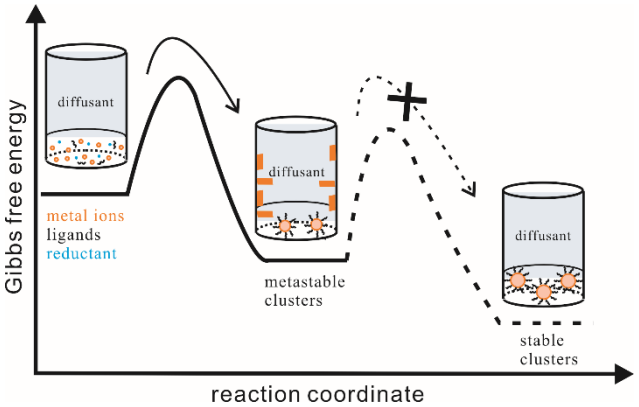

Figure 1. Reaction scheme in this work: metal precursor, ligand, and reducing agent were mixed together to form a homogeneous solution, a solvent (designated as diffusant), with a poor solubility for the cluster products, was layered over the reaction mixture (left). Once formation of metastable clusters, the species are trapped into diffusant solvents to form single crystals (middle), which stops further transformation to stable ones (right).

initial stage. Once formed, they were trapped in the diffusant to form single crystals (middle).

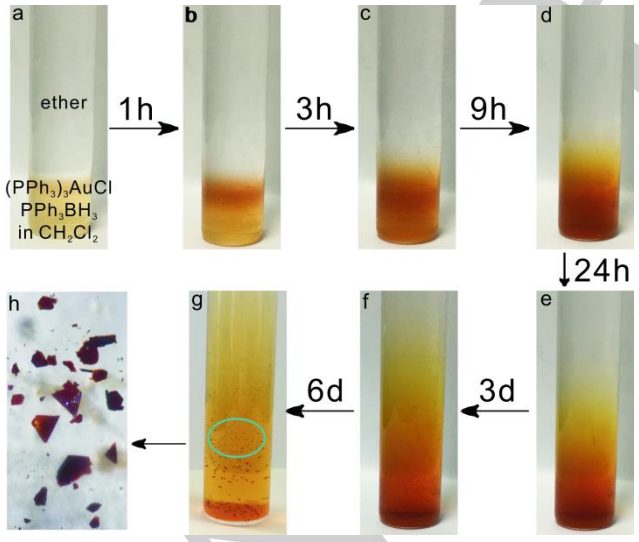

Figure 2. Representative photos of reaction solutions at different time. (a) $(PPh_3)_3AuCl$ and PPh_3BH_3 were dissolved together in mixed solvent of dichloromethane and methanol, above which ether was covered. (b-g) As time progresses, the solution turns from colorless, pale yellow, pale red, red, and dark red, respectively. (h) Red plate crystals formed on the tube.

Figure 2 depicts the experiment procedure guided by this principle. Typically, $(PPh_3)_3AuCl$ (precursor) and PPh_3BH_3 (reductant) were dissolved in a mixture of CH_2Cl_2 and MeOH with stirring to form a clear solution. Then another solvent, in the present case, ether, was layered over the reaction mixture (see Experimental Section for more details). As the reaction progressed, it was observed that the initial colorless solution turned pale red, red, dark red gradually (Figure 2b-2g), suggesting gold precursor was reduced to form clusters (Figure S2). Red plate crystals were formed on the tube wall in the ether layer after one week (Figure 2h). Yield: ca. 36% based on Au.

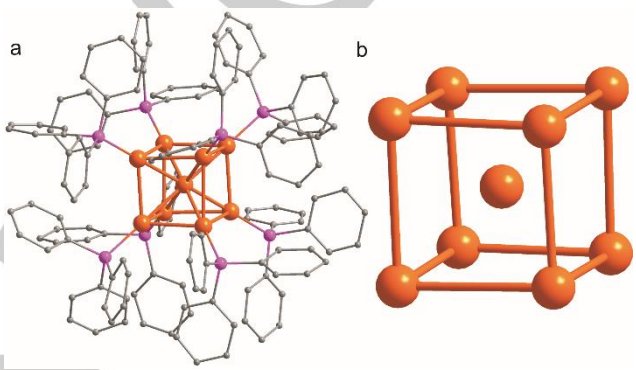

Figure 3. Crystal structure of **1**. (a) overall structure and (b) metal core. Color legend: orange spheres, Au; pink spheres, P; gray spheres, C. All hydrogen atoms are omitted for clarity.

Atomic and electronic structure of 1. The crystals of **1** were characterized by X-ray crystallographic analysis, which revealed that the cluster crystallizes in R-3 space group (Table S1) and the unit cell contains three clusters (Figure S3 and S4). Each cluster consists of 9 Au atoms, 8 triphenylphosphine ligands, giving rise to the overall formula of $[Au_9(PPh_3)_8]+$ (**1**). The metal core of **1** exhibits rare body-centered-cubic structure which is capped by eight phosphine ligands, one each at the eight vertices (Figure 3a). Detailed structural analysis shows that metal core of **1** displays a nearly perfect body-centered cubic structure (Figure 3b and S5). The average bond length and bond angles of Au atoms of the cube to be 3.021 Å and 89.995°, respectively (Figure S5-6 and Table S2-3). The average distance between centered Au atom and its surrounding 8 Au atoms is 2.616 Å. All phosphine ligands bind with Au atoms via single bond with average bond distance of 2.307 Å. We note that there are strong inter-molecular C-H•••π interactions between neighboring phosphine ligands (Figure S7), which probably supports the body-centered cubic (bcc) core of **1**. It is well known that face-centered-cubic (fcc) structure is inherent to bulk gold, thus atomic structures such as face-centered-cubic (fcc) and cuboctahedral arrangements are commonly observed in reported gold NCs. To the best of our knowledge, this is the first time that a gold NC with an unusual

10.1002/chem.202001753

bcc architecture was structurally determined. Recently, Jin and co-workers have synthesized a $Au_{38}S_2(S\text{-}Adm)_{20}$ NC with a bcc gold core via traditional reduction-aging-isolation strategy. However, in the latter case, the formation of bcc core was affected by rigid surface organic ligands.[16]

It should be noted that gold clusters with the same composition of $[Au_9(PR_3)_8]^{3+}$ (3, R=Ph or C_6H_4OMe) but different charges had been reported by Mingos et al. decades ago.[17] It has a metal skeleton displayed either butterfly or centered-crown structure, distinctly different from the bcc structure reported here. For $[Au_9(PPh_3)_8](NO_3)_3$, the average distance between centered Au atom and its surrounding 8 Au atoms is 2.6912 Å, comparable with that in **1**. The average peripheral Au-Au bond length of $[Au_9(PPh_3)_8](NO_3)_3$ (2.834 Å), however, is much less than that of **1** (3.021 Å). In the realm of basic polyhedron-based unit clusters, tetrahedral Au_4,[18] icosahedral Au_{13},[19] and face-center-cubic Ag_{14}[20] are well documented. To the best of our knowledge, this work is the first report of a standalone bcc Au_9 NC, fully characterized structurally.[21] Thus, the Au_9 reported here may be characterized as the smallest bcc cluster unit which may serve as the basic building block for larger clusters.

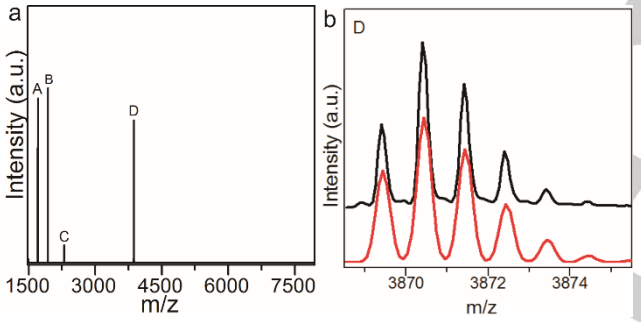

Figure 4. (a). ESI-MS spectrum of **1** single crystals in CH_2Cl_2. Peak D corresponds to cluster **1**, and other peaks A, B, and C indicate the fragment species $[Au_8(PPh_3)_7]^{2+}$, $[Au_9(PPh_3)_8]^{2+}$, and $[Au_7(PPh_3)_7]^{+}$ formed during the ESI process. (b) The experimental (black trace) and simulated (red trace) isotopic patterns of the $[Au_9(PPh_3)_8]^{+}$.

The composition of the cluster was confirmed by time of flight electrospray ionization mass (TOF−ESI−MS). As shown in Figure 4a, there is a prominent peak (D) at 3870 m/z, which corresponds to mono-cationic $[Au_9(PPh_3)_8]^{+}$. The simulated isotopic pattern of the peak is in perfect agreement with the experimental data (Figure 4b). Other peaks can be assigned to the fragments (e.g., $[Au_8(PPh_3)_7]^{2+}$ for peak A, $[Au_9(PPh_3)_8]^{2+}$ for peak B, $[Au_7(PPh_3)_7]^{+}$ for peak C) of the parental cluster formed during the ESI process (Figure S8), which is common for phosphine-protected gold clusters (Figure S9).[22] Phosphine ligands in **1** are in equivalent environments, as suggested by a singlet peak at 33.21 ppm in its ^{31}P NMR spectrum (Figure S10).

Electronic structure of 1.

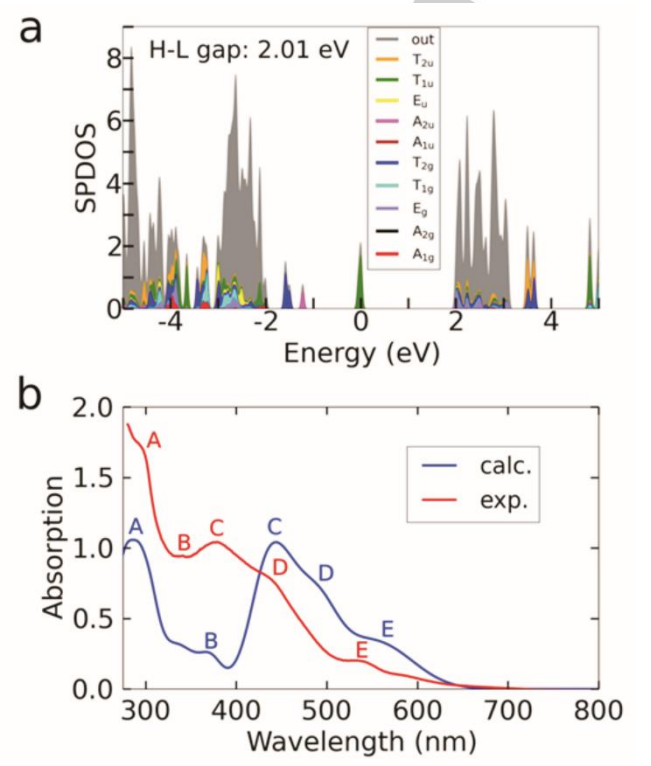

Figure 5. (a) The computed symmetry-projected density of electron states (SPDOS) of **1** as shown in the octahedral (O_h) symmetry group. The HOMO energy is set to zero. (b) Measured and computed UV/Vis spectra of **1**. The experimental spectrum was measured of crystals of **1** dissolved in CH_2Cl_2. Common features between spectra are indicated as A-E (see text). The computed spectrum is plotted without any shift in the wavelength axis, but the intensity is scaled to experimental spectrum such that the heights of the peaks "C" are the same. Individual optical transitions are smoothed by 0.1 eV Gaussians.

Density functional theory (DFT) calculations were performed to to provide details of the electronic structure and optical properties of **1**. The ground-state electronic structure was calculated directly for the experimental crystal structure by using the GLLB-SC exchange-correlation (xc) potential[23] (Supporting information). The electron count of **1** yields eight electrons indicating an electronic shell closing.[24] As shown in Figure 5a, cluster **1** indeed shows a large energy gap (GLLB-SC value of 2.01 eV) between the highest occupied (HOMO) and lowest unoccupied (LUMO) molecular orbitals. The HOMO orbitals are three-fold degenerate metal-centered orbitals showing T_{1u} symmetry in the octahedral point group, corresponding roughly to P-type orbitals in a spherical system (see visualizations of individual orbitals in Figure S11). Below the HOMO there is a set of four orbitals HOMO-3 to HOMO-6 showing A_{2u} and T_{2g} symmetries. These have significant weight also on gold-phosphorous bonds (Figure S11). Orbitals at

10.1002/chem.202001753

LUMO and above have significant weights in the ligand layer and less clear symmetries in the gold core.

Figure 5b shows the measured UV/Vis spectrum of **1** dissolved in dichloromethane. It exhibits several absorption features at 296 (A), 340 (B), 377 (C), 433 (D), 538 (E), and 588 nm, respectively. The theoretical UV/Vis spectrum, shown in Figure 5b, was computed by using the linear-response form of the time-dependent DFT (LR-TDDFT), GLLB-SC ground state wave functions, and the PBE functional[25] for the xc kernel. Both the measured and computed spectra show an apparent optical gap close to 620-630 nm, corresponding well to the computed HOMO-LUMO gap of 2.01 eV as discussed above. Although the absorption peaks in the computed spectrum appear red-shifted as compared to experiment, the shapes of both spectra agree very well and many common features (marked as A-E) can be identified. Analysis of the three lowest clear absorptions in the computed spectrum (peaks C, D, E in Figure 5b) by means of dipole transition contribution map (DTCM)[26] and electron-hole density (see Supporting information) shows that they are all metal-to-ligand type, where holes are created in the metal-centered HOMO manifold and electrons are transferred to ligand states (Figure S12). The lowest excitations are clearly over the HOMO-LUMO gap.

Metastability of 1. As a proof of concept, we performed an in situ time-dependent study of UV/Vis (Figure S13) and ESI-MS (Figure 6) of **1** to confirm its metastable nature. Single crystals of **1** were dissolved in CH_2Cl_2 for the time-dependent measurement. No obvious changes in the ESI-MS spectra of the

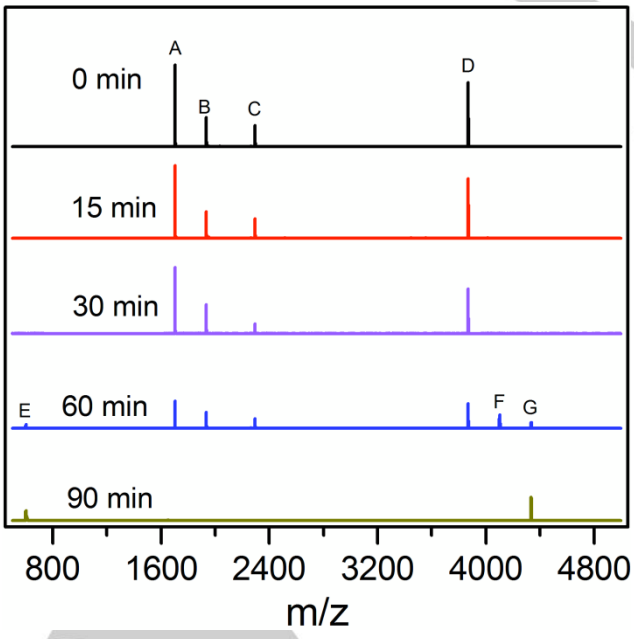

Figure 6. Real time tracking ESI-MS spectra of single crystals of **1** in dichloromethane at room temperature. Peaks A, B, C and D represent $[Au_9(PPh_3)_8]^+$ and its fragments; three new peaks, marked as E, due to $[Au(PPh_3)_3]^+$, F, due to $[Au_{10}(PPh_3)_8Cl]^+$, and G, due to $[Au_{11}(PPh_3)_8Cl_2]^+$ appeared after 60 min. At 90 min., only $[Au(PPh_3)_3]^+$ and $[Au_{11}(PPh_3)_8Cl_2]^+$ remained.

cluster were detected in the first 30 min. There was, however, an abrupt degradation of the major MS peaks after 30 min. The molecular peaks of $[Au_9(PPh_3)_8]^+$ practically disappeared, and in the meanwhile some other clusters such as $[Au(PPh_3)_3]^+$ (983 Da, peak E), $[Au_{10}(PPh_3)_8Cl]^+$ at the peak of 4104 (peak F) and $[Au_{11}(PPh_3)_8Cl_2]^+$ (**2**) at m/z=4335 (peak G) were formed in the solution (detailed analysis of peaks in Figure S14). As the reaction proceeded, the peak of E and G gradually increased, with the disappearing of all other peaks, indicating that **1** was eventually converted to **2**. The result of UV/Vis measurement is in good agreement with observation in ESI-MS (Figure S13). In the UV/Vis measurement, the spectroscopic profile of **1** was almost unchanged in the first 30 min. Thereafter, the features at 340, 433, 538 and 588 nm gradually disappeared, and some other peaks such as that at 433 nm emerged. Overall, from both ESI-MS and UV/Vis measurement, it can be inferred that **1** gradually transformed to $[Au_{10}(PPh_3)_8Cl]^+$, and finally to **2**. Based on abovementioned results, we hypothesize that the **1** would be an intermediate in the formation of **2**. We note that **1** is also metastable in other non-chloride solvents such as THF, as its UV/Vis profile changed significantly in 40 min (Figure S15). It occurs to us that **1** may be employed as an intermediate in the synthesis of other gold clusters. Although the same composition of $[Au_9(PPh_3)_8]^{3+}$ with **1**, $[Au_9(PPh_3)_8]^{3+}$ cannot transform to other clusters spontaneously in the same condition (Figure S16), confirming the metastable nature of **1**.

To rationalize these experimental observations, we performed additional DFT calculations on cluster **2**, taking the published crystal structure of $[Au_{11}(PPh_3)_8Cl_2]^+$ from the Hutchison group as the reference.[2] The total energy balance as calculated for PBE-relaxed structures **1** and **2** for stoichiometric reaction E[**2**] – E[**1**] – 2 E[AuCl] = -4.8 eV indicating a strong enthalpic driving force favoring cluster **2**. Additionally, the HOMO-LUMO gap (GLLB-SC value) of **2** is 2.23 eV as compared to 2.01 eV for **1** at the same level of theory. This indicates an additional stabilizing factor favoring cluster **2**. In fact, examination of the evolution of UV/Vis spectra in time in Figure S13 indicates that as cluster **1** transforms to **2**, the optical gap slightly increases, in good agreement with the results discussed above.

Shape isomers of $[Au_9(PR_3)_8]^q$ clusters. Finally, as discussed above, tri-cationic forms of the phosphine-protected nonagold cluster $[Au_9(PR_3)_8]^{+3}$ have been known for a long time. The metal core geometries of those clusters could be described as “butterfly-like” and they correspond to a six-electron system. The discovery

and precise structure determination of the cubic, mono-cationic, eight-electron cluster $[Au_9(PR_3)_8]^+$ in this work gives an interesting possibility to investigate computationally the connection between the cluster charge (i.e., the free-electron count six vs. eight), the shape of the metal core, and the total energy. To this end, we created four models M1-M4 for $[Au_9(PPh_3)_8]^q$, optimized their atomic structure by using the PBE DFT functional, and compared their shapes and total energies. Model M1 is the cluster **1** (q=+1) discovered in this work, M2 is the charge isomer (q=+3) obtained by relaxing M1 with q=+3. M3 is the cluster reported before by Simon and collaborators (q=+3) and M4 is the mono-cationic charge isomer of M3. Figure S17 shows the metal core structure (ligands not shown) of M1-M4, their computed principal moments of inertia I_{xx}, I_{yy}, I_{zz} (describing the shape of the core) and their total energies. As seen in Figure S17, the hypothetical six-electron cluster M2 obtained from cluster **1** deforms slightly toward an "oblate" shape ($I_{xx} < I_{yy} < I_{zz}$) as expected by reducing the number of free electrons from eight to six, but is still about 0.76 eV higher in total energy than the crystallographically known cluster M3. Obviously, an energy barrier exists involving a complete re-organization of M2 into the known cluster M3. The metal core of M3 is tri-axial (Ixx < Iyy < Izz) and it remains tri-axial also when the charge is reduced to +1 in M4. M4 is still about 0.21 eV higher in total energy than the crystallographically known M1. These results show that changes in the electronic structure (here induced by changes in charge) definitely create a driving force to change atom geometry; a phenomenon that has been long discussed in the physics of bare metal clusters studied in gas phase.[27] These theoretical results suggest that it could be possible to affect the structure by manipulating the cluster charge in the solution phase. Creation of such (redox) structural isomers could be important for deeper studies of cluster reactivity.

Conclusion

In conclusion, this work reports a novel synthetic approach for crystallization of metastable gold nanoclusters. The basic principle of this approach is "trapping by solubility." As an illustrative example, a nonagold cluster with nearly perfect body-centered-cubic structure was isolated and fully characterized. As revealed by ESI-MS and UV/Vis measurements, the nonagold cluster, $[Au_9(PPh_3)_8]^+$, converts to the well-known undecagold cluster $[Au_{11}(PPh_3)_8Cl_2]^+$ spontaneously in solution. As indicated by DFT calculation, the transformation is driven by an enthalpic gain and further stabilization of the electronic structure by an increased HOMO-LUMO energy gap of $Au_{11}(PPh_3)_8Cl_2]^+$ as compared to $[Au_9(PPh_3)_8]^+$. DFT also predicts that new structural isomers of ligand-stabilized clusters could be created by manipulating their electronic structure via controlling the overall charge. The metastable nature of **1** also provides an unprecedented opportunity to study transformation chemistry of metal clusters. More work on catalytic performance of **1**, and the extension of the synthetic protocol to other systems is ongoing in our laboratory. It is hoped that this work will stimulate more research towards controlled synthesis and characterization of other metastable metal nanoclusters.

Experimental Section

Synthesis of $[Au_9(PPh_3)_8]Cl$. *Method 1:* In a typical synthesis, 18.8 mg (0.055 mmol) $Al_2(SO_4)_3$•$18H_2O$ was dissolved in mixed solvent of CH_2Cl_2 and MeOH under sonication. To the solution was added 100 mg (0.38 mmol) PPh_3 as solid. After stirring the solution for 10 min, 34.5 mg (0.91 mmol) $NaBH_4$ in 1 ml ice-cold MeOH was added. The reaction was aged overnight to produce PPh_3BH_3 in-situ. To the solution was added 100 mg PPh_3AuCl (0.2 mmol). The solution was stirred for 2 min and filtered, above which was covered with ether. The solution turns from colorless, to pale red, to red. During the period of reducing process, red plate crystals were formed on the tube wall (36.6% yield, based on Au) after one week.

Method 2: The same result can be obtained by mixing $(PPh_3)_3AuCl$, PPh_3BH_3 and NH_4Cl in mixed solvent of CH_2Cl_2 and MeOH.

Transformation of $[Au_9(PPh_3)_8]Cl$: single crystals of $[Au_9(PPh_3)_8]Cl$ was dissolved in dichloromethane or THF at room temperature. With the time going, the sample was characterized with ESI-MS and UV/Vis measurement.

Acknowledgements

We thank the National Key R&D Program of China (2017YFA0207302) and the NSF of China (21890752, 21731005, 21721001) for financial support. The computational work in the University of Jyväskylä was supported by the Academy of Finland (grants 294217, 319208, 315549, and through HH's Academy Professorship). H.H. acknowledges support from China's National Innovation and Intelligence Introduction Base visitor program. E.S. acknowledges the Emil Aaltonen Foundation for a PhD study grant. The computations were made at the CSC supercomputing center in Finland and as part of a PRACE project in the Barcelona Supercomputing Center.

Keywords: body-centered cubic •gold • nanocluster • solubility-driven • metastable compounds

[1] a) P. X. Liu, R. X. Qin, G. Fu, N. F. Zheng, *J. Am. Chem. Soc.* **2017**, *139*, 2122-2131; b) J. Z. Yan, B. K. Teo, N. F. Zheng, *Acc. Chem. Res.* **2018**, *51*, 3084−3093; c) Y. Negishi, T. Nakazaki, S. Malola, S. Takano, Y. Niihori, W. Kurashige, S. Yamazoe, T. Tsukuda, H. Häkkinen, *J. Am. Chem. Soc.* **2015**, *137*, 1206-1212; d) R. Jin, C. Zeng, M. Zhou, Y. Chen, *Chem. Rev.* **2016**, *116*, 10346-10413; e) I. Chakraborty, T. Pradeep, *Chem. Rev.* **2017**, *117*, 8208−8271; f) Z. Lei, X. Wan, S. Yuan, Z. Guan, Q. Wang, *Acc. Chem. Res.* **2018**, *51*, 2465-2474; g) K. Konishi, M. Iwasaki, Y. Shichibu, *Acc. Chem. Res.* **2018**, *51*, 3125-3133.

[2] L. C. McKenzie, T. O. Zaikova, J. E. Hutchison, *J. Am. Chem. Soc.* **2014**, *136*, 13426-13435.

[3] Y. Shichibu, K. Konishi, *Small* **2010**, *6*, 1216-1220.

[4] B. K. Teo, X. Shi, H. Zhang, *J. Am. Chem. Soc.* **1992**, *114*, 2743-2745.
[5] M. Zhu, C. Aikens, F. Hollander, G. Schatz, R. Jin, *J. Am. Chem. Soc.* **2008**, *130*, 5883–5885.
[6] P. Jadzinsky, G. Calero, C. Ackerson, D. Bushnell, R. Kornberg, *Science* **2007**, *318*, 430-433.
[7] N. Yan, N. Xia, L. Liao, M. Zhu, F. Jin, R. Jin, Z. Wu, *Sci. Adv.* **2018**, *4*, eaat7259.
[8] J. J. Li, Z. J. Guan, Z. Lei, F. Hu, Q. M. Wang, *Angew. Chem. Int. Ed.* **2019**, *58*, 1083-1087.
[9] Z. Lei, J. Li, X. Wan, W. Zhang, Q. Wang, *Angew. Chem. Int. Ed.* **2018**, *57*, 8639-8643.
[10] M. R. Narouz, S. Takano, P. A. Lummis, T. I. Levchenko, A. Nazemi, S. Kaappa, S. Malola, G. Yousefalizadeh, L. A. Calhoun, K. G. Stamplecoskie, H. Häkkinen, T. Tsukuda, C. M. Crudden, *J. Am. Chem. Soc.* **2019**, *141*, 14997-15002.
[11] H. Shen, G. C. Deng, S. Kaappa, T. D. Tan, Y. Z. Han, S. Malola, S. C. Lin, B. K. Teo, H. Häkkinen, N. F. Zheng, *Angew. Chem. Int. Ed.* **2019**, *58*, 2-7.
[12] P. Pattekari, Z. Zheng, X. Zhang, T. Levchenko, V. Torchilin, Y. Lvov, *Phys. Chem. Chem. Phys.* **2011**, *13*, 9014-9019.
[13] a) R. Jin, H. Qian, Z. Wu, Y. Zhu, M. Zhu, A. Mohanty, N. Garg, *J. Phys. Chem. Lett.* **2010**, *1*, 2903-2910; b) Y. Negishi, K. Nobusada, T. Tsukuda, *J. Am. Chem. Soc.* **2005**, *127*, 5261-5270; c) Z. Wu, M. A. MacDonald, J. Chen, P. Zhang, R. Jin, *J. Am. Chem. Soc.* **2011**, *133*, 9670-9673.
[14] R. Sardar, P. J. S. Shumaker, *J. Am. Chem. Soc.* **2011**, *133*, 8179-8190.
[15] Q. Yao, T. Chen, X. Yuan, J. Xie, *Acc. Chem. Res.* **2018**, *51*, 1338-1348.
[16] C. Liu, T. Li, G. Li, K. Nobusada, C. Zeng, G. Pang, N. Rosi, R. Jin, *Angew. Chem. Int. Ed.* **2015**, *54*, 9826-9829.
[17] a) C. E. Briant, K. P. Hall, D. M. P. Mingos, *J. Chem. Soc. Chem. Commun.* **1984**, 290-291; b) F. Wen, U. Englert, B. Gutrath, U. Simon, *Eur. J. Inorg. Chem.* **2008**, *2008*, 106-111.
[18] E. Zeller, H. Beruda, H. Schmidbau, *Inorg. Chem.* **1993**, *32*, 3203-3204.
[19] C. E. Briant, B. R. C. Theobald, J. W. White, L. K. Bell, D. M. P. Mingo, *J. Chem. Soc. Chem. Commun.* **1981**, 201-202.
[20] H. Y. Yang, J. Lei, B. H. Wu, Y. Wang, M. Zhou, A. D. Xia, L. S. Zheng, N. F. Zheng, *Chem. Commun.* **2013**, *49*, 300-302.
[21] a) J. G. M. Linden, M. L. H. Paulissen, J. E. J. Schmitz, *J. Am. Chem. Soc.* **1983**, *105*, 1903-1907; b) J. W. A. Velden, J. J. Bour, W. P. Bosman, J. H. Noordik, P. T. Beurskens, *Recl. Trav. Chim. Pays-Bas* **1984**, *103*, 13-16.
[22] a) S. Takano, H. Hirai, S. Muramatsu, T. Tsukuda, *J. Am. Chem. Soc.* **2018**, *140*, 8380-8383; b) X. K. Wan, Z. W. Lin, Q. M. Wang, *J. Am. Chem. Soc.* **2012**, *134*, 14750-14752; c) R. Tomihara, K. Hirata, H. Yamamoto, S. Takano, K. Koyasu, T. Tsukuda, *ACS Omega* **2018**, *3*, 6237-6242.
[23] M. Kuisma, J. Ojanen, J. Enkovaara, T. T. Rantala, *Phys. Rev. B* **2010**, *82*, 115106.
[24] M. Walter, J. Akola, O. L. Acevedo, P. D. Jadzinsky, G. Calero, C. J. Ackerson, R. L. Whetten, H. Gronbeck, H. Häkkinen, *Proc. Natl. Acad. Sci.* **2008**, *105*, 9157-9162.
[25] J. Perdew, K. Burke, M. Ernzerhof, *Phys. Rev. Lett.* **1996**, *77*, 3865-3868.
[26] a) S. Malola, L. Lehtovaara, J. Enkovaara, H. Häkkinen, *ACS Nano* **2013**, *7*, 10263-10270; b) T. P. Rossi, M. Kuisma, M. J. Puska, R. M. Nieminen, P. Erhart, *J. Chem. Theory Comput.* **2017**, *13*, 4779-4790.
[27] H. Häkkinen, M. Manninen, *Phys. Rev. B* **1995**, *52*, 1540-1543.

10.1002/chem.202001753

WILEY-VCH

RESEARCH ARTICLE

A standalone nonagold cluster with exceptional body-centered cubic structure was isolated. The cluster is high reactive, as its spontaneous conversion to other species during short time. The metastable cluster was crystallized out successfully via a finely-designed reactor in which reduction and crystallization process take place in the meanwhile.

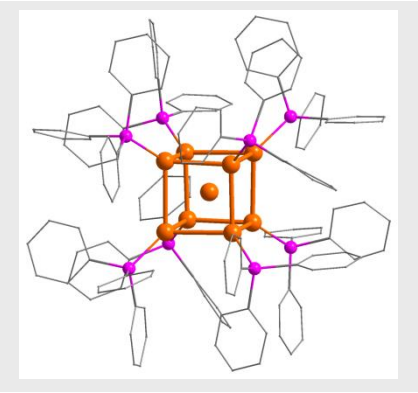

H. Shen, E. Selenius, P. Ruan, X. Li, P. Yuan, O. Lopez-Estrada, S. Malola, S. C. Lin, B. K. Teo, H. Häkkinen, N. F. Zheng**

Page No. – Page No.

Solubility-Driven Isolation of a Metastable Nonagold Cluster with Body-Centered Cubic Structure